2018

Void Fraction and Flow Regimes Determined by Visualization, Mass Measurement and New Capacitance Sensor

Hongliang Qian
UIUC, United States of America, hqian7@illinois.edu

Predrag S. Hrnjak
pega@illinois.edu

Void Fraction and Flow Regimes Determined By Visualization, Mass Measurement and New Capacitance Sensor

Hongliang Qian[1], Pega Hrnjak[1, 2]*

[1] Air Conditioning and Refrigeration Center, University of Illinois at Urbana-Champaign, 1206 West Green Street, Urbana, IL 61801, USA

[2] Creative Thermal Solutions, 2209 Willow Rd., Urbana, IL, USA

* Corresponding author: pega@illinois.edu +1-217-390-5278

ABSTRACT

This paper presents void fraction and flow regimes determined by three methods: visualization (high speed camera), mass measurement (quick-closing valves) and a newly developed capacitance sensor. In a way, this is a calibration process for a capacitance sensor. It is shown that new sensor can characterize flow patterns in low mass flux range and measure void fraction for horizontal and vertical tubes. A calibration procedure of void fraction measurement is based on a mass measurement (quick-closing valves). Two calibration curves for measuring void fraction in horizontal and vertical tubes are developed. With calibration curves, sensors with similar configurations can be directly utilized to measure void fraction in further studies.

1. INTRODUCTION

Void fraction which is defined as vapor phase volume over the total volume has been widely studied both theoretically and experimentally during the past several decades. Some methods including quicking-closing valves (Beggs, 1973, Koyama *et al.*, 2004, Yashar *et al.*, 2001), capacitance sensor (De Kerpel *et al.*, 2013, S. P. Olivier *et al.*, 2016), γ-ray absorption (Isbin *et al.*, 1957, Schmidt *et al.*, 2008) and optical (Wojtan *et al.*, 2004, 2005) are commonly used to measure void fraction in experiments. Optical visualization, mass measurement and capacitance sensors are also used to determine flow patterns for two-phase flow. Keska *et al.* (1999) suggested that capacitive signals showed very good potential to recognize flow patterns. Many researchers (Abouelwafa and Kendall, 1980, Ahmed and Ismail, 2008, Hugo Canière, T'Joen, *et al.*, 2007, Hugo Canière *et al.*, 2008, Elkow and Rezkallah, 1996, Geraets and Borst, 1988, Jaworek and Krupa, 2004, 2010, Kendoush and Sarkis, 1995) designed capacitance sensors to measure void fraction and detect flow regime for two-phase flows. Some typical electrode configurations of capacitance sensors on a round tube are shown in Figure 1. The two-concave plates' configuration (Figure 1a) is chosen in this paper. This is because this configuration gives the sensor possibilities to measure local (cross-sectional) void fraction when reducing the axial length of electrodes. Due to the non-uniformity of the electrical field between the electrodes, a calibration procedure is necessary when applying capacitance sensors to measure void fraction.

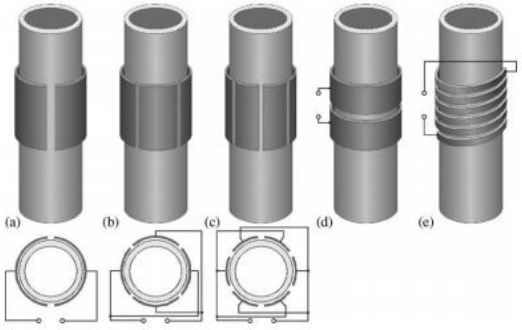

Figure 1 some typical electrode configurations. (a) Two concave plates. (b) Four concave plates. (c) Six concave plates. (d) Rings. (e) Double helix. (Jaworek and Krupa, 2004)

2. CAPACITANCE SENSOR DESIGN AND BUILDING

In this paper, the working fluid is R134a, which possess very high resistivity. Conductivity and dielectric constant for some other working media is shown in Table 1. Capacitive methods which neglects conductivity effects is thus used.

Table 1 Conductivity and dielectric constant for some working media (ASHRAE, 2013)

Working media	Volume Resistivity (MΩ/m)	Dielectric constant (-)
Air (0ºC)		1.00059
Pure water (25ºC) (Haynes, 2014)	0.182	79.55
R134a liquid at ambient temperature	17700	9.51
R134a liquid at 77ºF		9.87
R134a vapor at 77ºF		1.0125

The dielectric constant of water at 25ºC is much larger than that of R134a at the ambient temperature. In addition, the dielectric constant difference between water and air is much bigger than that between R134a liquid phase and vapor phase. As a result, overall capacitive signal difference got between full liquid phase and full vapor phase of R134a is smaller. The capability of the sensor to measure small capacitive signals (signals are typically in pF) should be achieved. The dielectric constant is a temperature dependent property. For R134a, several researches (Feja, 2012, Sedrez and Barbosa, 2015) reported dielectric constant decreased as temperature increased. The change of dielectric constant will affect capacitance measured from R134a two-phase flow. However, if the temperature is kept constant, this effect can be eliminated. This situation can be obtained when refrigerant is evaporating or condensing in the two-phase zone or refrigerant flows in a condition where no heat transfer occurs, like headers of microchannel heat exchangers. If the temperature various and cannot be kept constant, dos Reis and Goldstein (2005) developed a procedure to correct the effect of fluid flow temperature variation.

2.1 Determination of key parameters

The capacitance sensor used in this paper base on the work developed by Hugo Canière *et al.* (2007). Some modifications and further developments are made to this sensor so that it can be suitable for more configurations other than only horizontal tubes. In this paper, firstly, the new modified sensor is used to characterize flow patterns in both horizontal and vertical flows in smooth tubes. Next, a calibration procedure is proposed to measure void fraction based on experimental data. After that, the application of this sensor is extended to measure void fraction along headers of microchannel heat exchangers (to be presented in further publications).

Figure 2 shows the cross-sectional and side view of the capacitance sensor. Some key parameters need to be determined during the sensor design: dielectric layer thickness t, electrodes angle β, shield diameter R, orientation of the electrodes for horizontal configuration and axial electrode length L.

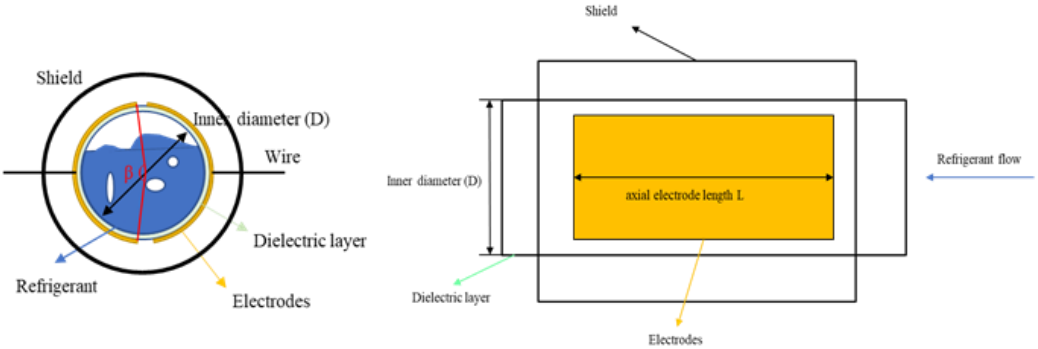

Figure 2 Cross-sectional and side view of the capacitance sensor

To obtain a higher homogeneity for the electric filed within the sensor and larger overall capacitance difference between full liquid phase and full vapor phase, H Canière (2010) reported *smaller shield radius, thinner dielectric layer thickness, larger electrode angle for the sensor and perpendicular towards gravity as the orientation of electrodes for horizontal configuration* should be applied. Some similar simulations to the work from H Canière (2010)

are made, and the results agree well to his. For axial electrode length, H Canière (2010) selected L which equaled one inner diameter (D) and claimed it could be further reduced if the transmitter could be improved. Three pairs of electrodes with axial length of one inner diameter (D), 2D/3 and D/2 are tested and presented in this paper. Results for the electrodes length of D/2 only will be reported in this paper. Comparison of signals from the three pairs of electrodes with different axial lengths mentioned above on characterizing flow patterns and measuring void fraction will be discussed in further study. From the discussion above, Table 2 lists the most important parameters of the capacitance sensor.

Table 2 Dimensions of key parameters

Key parameter	Dimension
Inner tube diameter, D	7 mm
Electrode axial length, L	D, 2D/3, D/2 (discussed)
Electrode angle, β	160º
Dielectric layer thickness, t	0.05 mm
Shield inner diameter, R	42.8 mm

2.2 Building of capacitance sensor

The dielectric layer and electrodes are made up with a laminate circuit material. Precise shapes and locations of electrodes on dielectric layer is achieved by the etching technique: A photomask with desired pattern of electrodes is first made. After developing the photoresist pattern onto the surface, etching is applied to eliminate other parts of copper. Seven pairs of electrodes (1-7) with three different axial lengths locate in a row (Figure 3). The gap between each pair of electrodes is half diameter (D/2). First three pairs from the left (1-3) have the axial length of one diameter (D). The axial length of the two pairs of electrodes in the middle (4 and 5) is 2D/3 and of the last two pairs (6 and 7) is D/2.

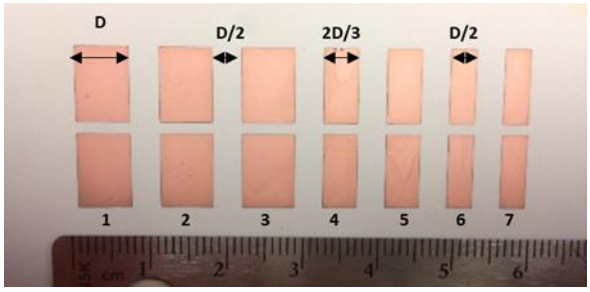

Figure 3 Configuration of the electrodes

After making this dielectric layer into a tube with a certain diameter, copper wires are then soldered onto the electrodes. Four pairs of electrodes (1, 3, 5 and 7) are connected to the ground as guarding electrodes which is to reduce the fringing effect and let the electric field be kept within the electrodes. The other three pairs with different axial length measure the capacitive signals within the electric field. 3D printed parts are mounted outside of this tube to support the structural stability. Outside of the inner design of the sensor, a piece of aluminum tube which is connected to the ground is used as a shield. This shield is to reduce outside influence like people moving or mobile signals. The gap between the 3D printed parts and the aluminum tube is filled with resin. The resin acts like a shield as well as ensures the sensor to withstand higher pressure. Figure 4 shows the final schematic of the capacitance sensor.

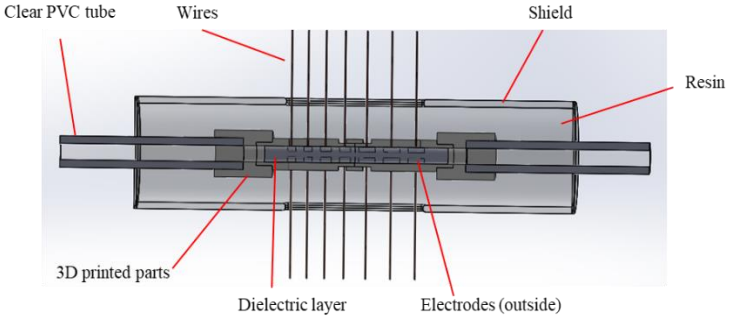

Figure 4 Capacitance sensor

The capacitive signals that the sensors measure are in the order of pF. Hence, the transmitter must be capable to measure such small capacitive signals and have reasonable high resolutions. Many researchers designed and built their

own transducers and transmitters based on several techniques: charge/discharge technique (H Canière, 2010, Hugo Canière, T'Joen, *et al.*, 2007, Hugo Canière *et al.*, 2008, Elkow and Rezkallah, 1996), frequency deviation (Jaworek and Krupa, 2004, Jaworek *et al.*, 2004) and phase shift (Jaworek and Krupa, 2010). Some devices are designed to measure air-water two-phase mixtures and may not be suitable for refrigerant flows due to the electric property difference mentioned above. H Canière (2010) developed a transducer for refrigerant flow that can measure capacitive signals in 0-10 pF range. However, this design is not open in the literature. This transducer is hard to be duplicated in other research groups and instrumental uncertainties may be introduced among transducers built by different groups. We have used a commercially available transmitter which can directly measure capacitive signals from custom sensors. It is capable to read such small capacitive signals and provide relative good resolution (approx. 0.001 pF).

3. FACILITY

The schematic drawing of the facility used is shown in Figure 5. Subcooled liquid refrigerant (R134a) is pumped through a mass flow meter with a gear pump into an electric heater where refrigerant is transformed into superheated vapor. Refrigerant is mixed in the mixer and the condition of refrigerant is determined by measuring its pressure and temperature. Then superheated vapor refrigerant flows into a pre-cooler whose secondary fluid is water. Water is cooled by building chilling water (7°C). With the energy balance of the water side in pre-cooler, the condition of refrigerant after the pre-cooler is determined. The model of pressure transducers is Setra 204 and thermocouples are T-type. The test section includes two quick closing valves (ball valves, manually open and close), the capacitance sensor and a visualization part. Figure 6 shows the schematic drawings for horizontal and vertical test sections. The visualization part is a piece of schedule 80 clear PVC tube with inner diameter of 7 mm. Before the visualization section, 600 mm (~86 diameters) of the same PVC tube for the horizontal configuration and 170 mm (~25 diameters) for the vertical configuration is utilized to ensure the flow is fully developed. In addition, for the vertical configuration, 460 mm of tube is maintained before the lower quick-closing valve to eliminate liquid pools within the test section. A high-speed camera is used to capture high-speed video of flow regimes with resolution 512x512 and speed of 2200 frames per second. Phantom CV 2.8 from Vision Research Inc. is used to process the video. The PVC pipe and two ball valves are connected by copper tubes whose inner diameter is 7 mm. The length of test section between two quick closing valves is 1500 mm (~214 diameters) for the horizontal configuration and 750 mm (~107 diameters) for the vertical configuration. Longer test section cannot be achieved due to the space limitation. A bypass loop is parallel to the test section. After the refrigerant passes test section, an after-cooler and a sub-cooler cool the refrigerant into subcooled liquid condition, which is fed into the gear pump to finish the loop.
Table 3 lists the experimental conditions and Table 4 lists uncertainties of the instruments.

Table 3 Experimental conditions

Working media	R134a
T_r	33ºC
Test section orientation	Horizontal and vertical
Test section length	Horizontal: 1500 mm (~214 dia.) Vertical: 750 mm (~107 diameters)
Mass flux	Horizontal: 40, 80 and 115 kg/m^{2}s Vertical: 65, 80 and 115 kg/m^{2}s
Quality	0.05-0.9

Table 4 Uncertainties of the instruments

Measurement point	Variable	Instrument	Uncertainty
Refrigerant and water temperature	T_r, T_w	T-type thermocouple	±0.5 K
Absolute pressure in the mixer and after the test section	P	Absolute pressure transducer (Setra 204)	±0.073% FS (±2.5 kPa)
Refrigerant mass flow rate	m_r	Coriolis mass flow meter	±0.1 g/s
Refrigerant weight	M	Scale (calibrated)	±0.1 g

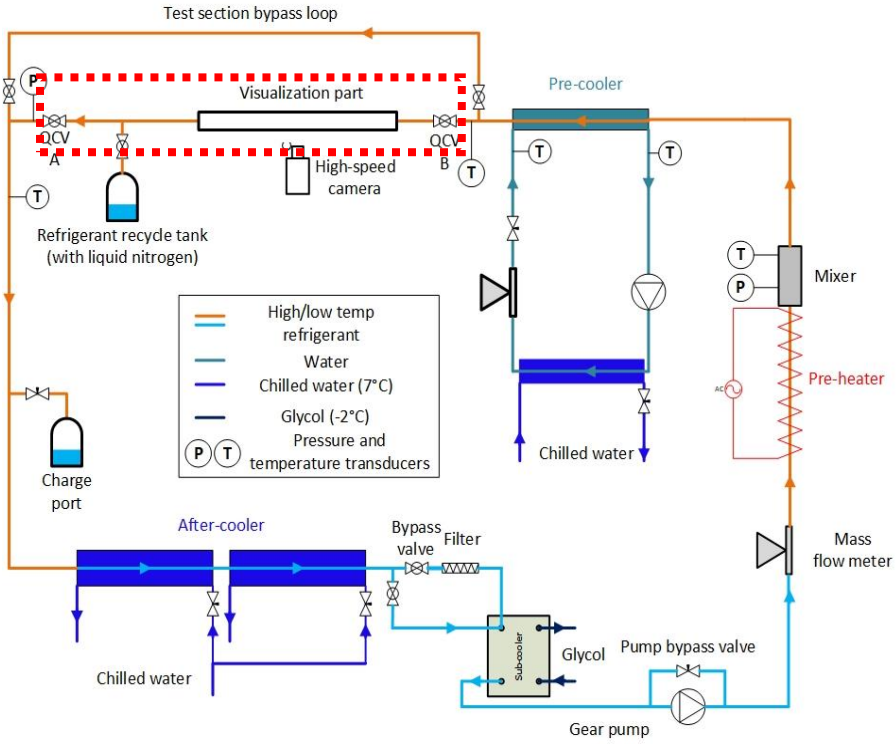

Figure 5 Schematic drawing of experimental facility, test section in the red box

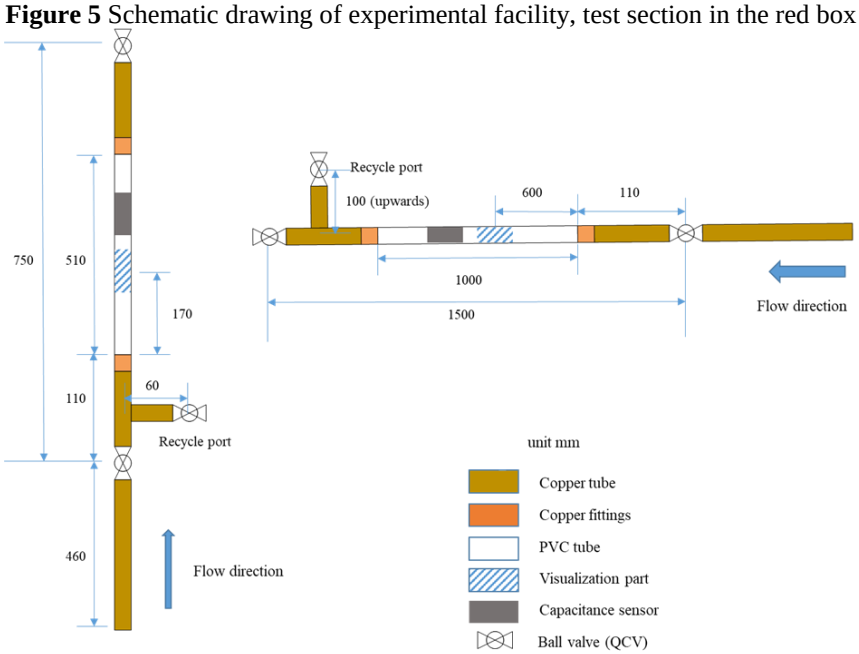

Figure 6 Schematic drawing for horizontal and vertical test section

For each test condition, the capacitive signals are read by the transmitter in pF directly. Before each set of experiments was conducted, capacitive signals for two base points are measured. The first is the capacitive signals for full vapor phase (C_{Vapor}) in the test section and the second is full liquid phase (C_{Liquid}). C_{Liquid} is obtained at 33 ºC, which is constant to T_r. S. Olivier *et al.* (2015) indicates dielectric constant of refrigerant vapor phase is not dependent on temperature. Hence, C_{Vapor} is measured at room temperature. After the two base points are measured, the capacitive signals for other test conditions ($C_{Measured}$) is then obtained. Normalized capacitance is then defined as following:

$$C_{norm} = \frac{C_{measured} - C_{Vapor}}{C_{Liquid} - C_{Vapor}} \quad (1)$$

The denominator which is assumed constant for the duration of the one set of experiments shows the entire range of signal change from two base points: $\Delta C_{L\text{-}V} = C_{Liquid} - C_{Vapor}$. The numerator shows the signals is how much larger than the full vapor condition. Hence, the normalized signals are typically from 0 to 1. Though C_{Liquid} and C_{Vapor} may shift among different sets of experiments, $\Delta C_{L\text{-}V}$ of different sets of experiments keeps quite constant as the temperature in the test section keeps constant (Table 5). De Kerpel *et al.* (2013) proposed that normalized calibration curves would not be affected if $\Delta C_{L\text{-}V}$ remained the same.

Table 5 range of $\Delta C_{L\text{-}V}$ for different sets of experiments for horizontal and vertical configurations, electrodes length L=D/2

	$\Delta C_{L\text{-}V}$ (pF)
Horizontal	1.118583304±0.057
Vertical	1.318990399±0.011

4. RESULTS

4.1 Capacitive signal characteristics for horizontal flow patterns

Two major flow patterns are observed with a high-speed camera for horizontal flows at the mass flux range studied in this paper: slug/stratified-wavy flow and stratified–wavy flow. Criteria for each flow pattern are listed below.

Slug/stratified-wavy flow: vapor slug appears in the upper portion of the tube periodically with liquid bridges in the middle. Boundary between upper vapor and lower liquid is wavy.

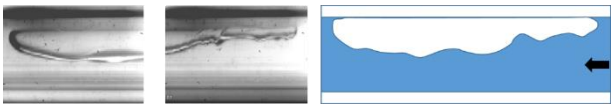

Figure 7 Slug/stratified-wavy flow (R134a, 80 kg/m^{2}s, x=0.1, T=33ºC)

Stratified-wavy flow: liquid flows at the bottom and vapor is in the upper portion of the tube. The interface is wavy, and no liquid bridges fills the entire cross section.

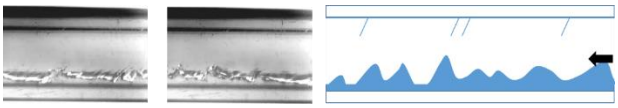

Figure 8 Stratified-way flow (R134a, 115 kg/m^{2}s, x=0.6, T=33ºC)

Figure 9 shows the normalized signals of slug/stratified-wavy flow (x=0.1), stratified-wavy flow (x=0.5) and two reference quality: fully liquid (x=0) and fully vapor (x=1) for the mass flux equals to G=80 kg/m^{2}s. For the slug/stratified-wavy flow (x=0.1), the signals show two concentrations at two major levels: one at the top and the other one in the middle. When the liquid bridges come into the sensor (liquid phase is filled in the entire cross-sectional area), the singles jump to 1. When vapor slugs come into the sensor, the signals stay at the lower level. Unlike the signals for x=0.1, signals of x=0.5 only concentrate at one major level. Signals fluctuate at a relatively suitable state and no huge oscillations are observed. For stratified-wavy flow in the visualization results, the interface between liquid phase and vapor phase is relatively constant with periodic waves. Figure 10 shows the probability density estimate (PDE) results for both x=0.1 and 0.5. PDE which is to estimate the probability density in a non-parametric way is used to obtain signal amplitude distributions. For PDE results of x=0.1, two peaks which represent dominant signal values are shown in this diagram. The first one is around one and the second is around 0.65. For results of x=0.5, only one steep peak is shown. Combing Figure 9 and 10, flow patterns in horizontal tubes in this mass flux range can be determined by capacitive signals.

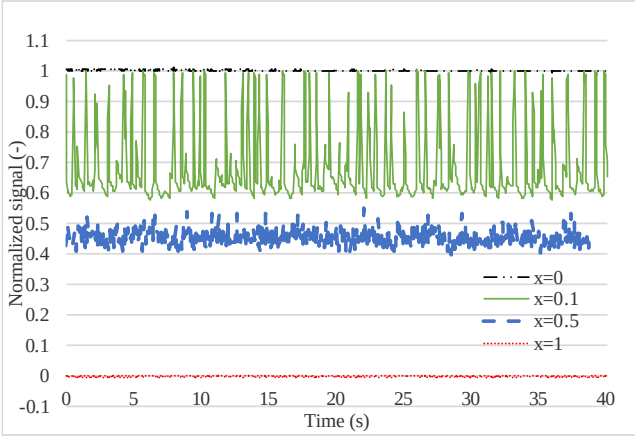

Figure 9 Normalized signals for x=0.1, x=0.5 and two base points, G=80 kg/m^{2}s, horizontal

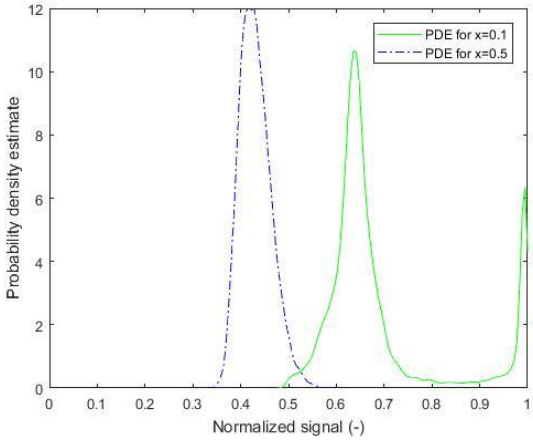

Figure 10 PDE for x=0.1 and x=0.5, G=80 kg/m^{2}s, horizontal

4.2 Capacitive signal characteristics for vertical upward flow patterns

For the flow upwards in vertical configuration, a high-speed camera is also used to capture flow patterns. Unlike in horizontal orientation, we observed slug, churn, and annular patterns. Criteria for each flow regime are listed below:

Slug flow: vapor slugs appear periodically with liquid bridge in the middle. The slugs are in the middle of the tube and filling almost the entire cross section due to the direction of gravity is opposite of the flow.
Annular flow: liquid flows along the wall of the tube with vapor in the central core. It is relatively more stable and less chaotic than churn flow though the interface between liquid and vapor core is wavy.

Churn flow: the total effect combined of shear on interface, pressure gradient and gravity on a droplet is not constant upwards. This results in chaotic structure of the flow: liquid may go up and down intermittently though the mean velocity of the two-phase mixture points up. This flow pattern is highly agitated and the interface between liquid and vapor is hard to locate.

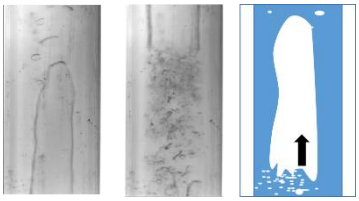

Figure 11 Slug flow (R134a, 80 kg/m^{2}s, x=0.1, T=33ºC)

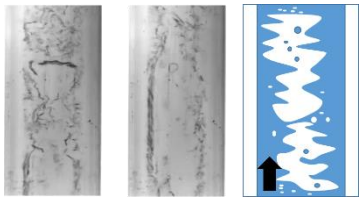

Figure 12 Churn flow (R134a, 80 kg/m^{2}s, x=0.5, T=33ºC)

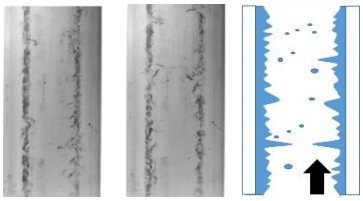

Figure 13 Annular flow (R134a, 115 kg/m^{2}s, x=0.9, T=33ºC)

Figure 14 shows the normalized signals of slug flow (x=0.1), churn flow (x=0.4), annular flow (x=0.8) and two reference conditions: x=0 and x=1 for mass flux equals to g=80 kg/m^{2}s. For slug flow, the signal pattern is similar to slug flows in horizontal tubes. The signals concentrate at two major levels: one at the top and the other at the middle. The singles jump to 1 when the liquid bridges come into the sensor and stay at the lower level when vapor slugs come into the sensor. For annular flows, the signals concentrate at one major level. Signals fluctuate at a relatively suitable state and no huge oscillations are observed. In the visualization results, liquid flows along the wall of tubes and vapor in the central core. No liquid bridges or huge waves are observed. Signals for churn flows are relatively more unstable compared to annular flows. The amplitude of oscillation is bigger. Figure 15 shows the PDE results of the three test conditions mentioned above. Two peaks which represent dominant signal values are shown for slug flows. Only one peak which represents the dominant signal value is shown for annular flows. The peak in the diagram has a very small span, which shows the possibility of signals appears closely around the major value is much higher than other ranges. For churn flows, only one peak shows in the diagram as well. However, the span of the peak is bigger than that of annular flow, which means signals appear in a wider range.

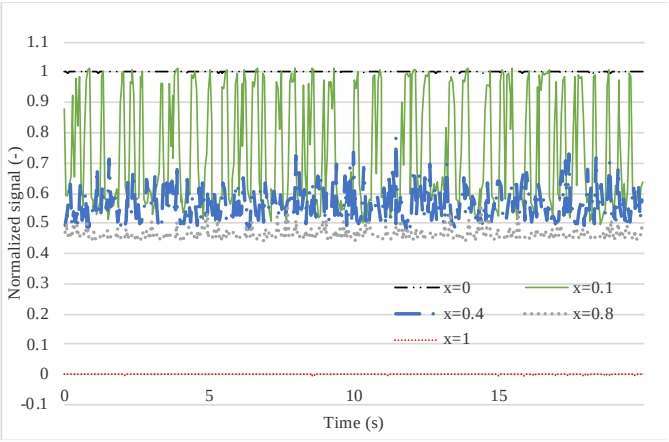

Figure 14 Normalized signals for x=0.1, x=0.4, x=0.8 and two base points, G=80 kg/m^{2}s, vertical

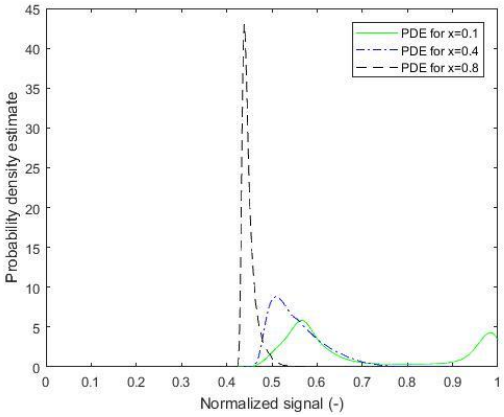

Figure 15 PDE for x=0.1, x=0.4 and x=0.8 G=80 kg/m^{2}s, vertical

4.3 Calibrated correlations for void fraction based on mass measurements in horizontal tubes

Due to the non-uniform electric field between two concave electrodes, the capacitive signals are dependent on both void fraction and phase distribution. Hence, the relation between time-averaged signals and void fraction are not linear. To measure refrigerant two-phase flow void fraction, the capacitance sensor must be calibrated first. In this paper, quick-closing valves which are located on both ends of the test section are used for each test condition. After the system becomes stable (temperature, pressure and quality are kept constant and flow in the test section is fully developed), collect capacitive signals for a relative sufficient long period of time and record the pattern with a high-speed camera. Then with quick-closing valves and refrigerant removing with liquid nitrogen, the void fraction is obtained. The curve fitting shows the relation between normalized capacitive signal and void fraction for horizontal flow and vertical upward flow in this mass flux range (Figure 16). Different flow pattern regions and mass fluxes mentioned above are marked in this map. With this curve, sensors with the same configuration can be directly utilized to measure void fraction in horizontal flows and vertical upward flows with R134a in this mass flux range.

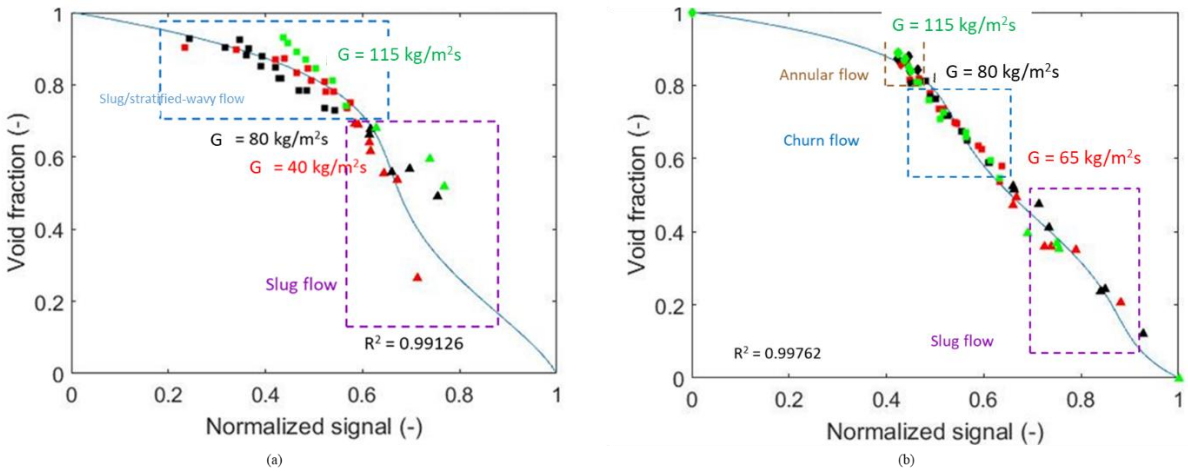

Figure 16 Calibrated relationship for capacitance sensor: measured void fraction by extraction vs. normalized signal at low mass flux, R134a, 33ºC.
(a) horizontal flows; (b) vertical upward flows

5. CONCLUSIONS

Void fraction and flow regimes are studied by three methods in this paper: visualization (high speed camera), mass measurement (quick-closing valves) and a newly developed capacitance sensor. The design and building of new capacitance sensor based on the work from Hugo Canière, T'Joen, *et al.* (2007) are discussed. Some modifications

and further developments are made to this sensor so that it can be suitable for more configurations. With normalized signals and PDE results corresponding to visualization from a high-speed camera, the sensor has the capability to characterize different flow patterns of both horizontal and vertical flows. A calibration procedure of void fraction measurement which is based on a mass measurement (quick-closing valves) – not correlations is proposed. Two calibration curves for measuring void fraction in horizontal and vertical tubes are developed. With calibration curves sensors with similar configurations is directly utilized to measure void fraction now and in further studies.

NOMENCLATURE

C	Capacitance signals	(pF)
D	Inner tube diameter	(mm)
G	Mass flux	(kg/m^2s)
L	Axial electrode length	(mm)
P	Absolute pressure	(kPa)
R	Shield inner diameter	(mm)
t	Dielectric layer thickness	(mm)
x	Vapor quality	(–)
α	Void fraction	(–)
ρ	Density	(kg/m^3)
σ	Surface tension	(N/m)

Subscript

V/Vapor	Vapor phase
L/Liquid	Liquid phase
L-V	Difference between fully liquid and fully vapor
NORM	Normalized
r	Refrigerant
w	Water

REFERENCES

Abouelwafa, M. S. A., & Kendall, E. J. M. (1980). The use of capacitance sensors for phase percentage determination in multiphase pipelines. *IEEE Transactions on Instrumentation and measurement, 29*(1), 24-27.

Ahmed, W. H., & Ismail, B. I. (2008). Innovative techniques for two-phase flow measurements. *Recent Patents on Electrical & Electronic Engineering (Formerly Recent Patents on Electrical Engineering), 1*(1), 1-13.

ASHRAE. (2013). 2013 ASHRAE Handbook - Fundamentals (I-P Edition). In: American Society of Heating, Refrigerating and Air-Conditioning Engineers, Inc.

Beggs, H. D. (1973). An experimental study of two-phase flow in inclined pipes.

Canière, H. (2010). Flow Pattern Mapping of Horizontal Evaporating Refrigerant Flow Based on Capacitive Void Fraction Measurements (Ph. D. thesis) Ghent University. *Ghent University*.

Canière, H., T'Joen, C., Willockx, A., De Paepe, M., Christians, M., Van Rooyen, E., . . . Meyer, J. (2007). Horizontal two-phase flow characterization for small diameter tubes with a capacitance sensor. *Measurement Science and Technology, 18*(9), 2898.

Canière, H., T'Joen, C., Willockx, A., & De Paepe, M. (2007). *Capacitance Sensor Design For Refrigerant Two-Phase Flow Characterization.* Paper presented at the AIP Conference Proceedings.

Canière, H., T'Joen, C., Willockx, A., & De Paepe, M. (2008). Capacitance signal analysis of horizontal two-phase flow in a small diameter tube. *Experimental Thermal and Fluid Science, 32*(3), 892-904.

De Kerpel, K., Ameel, B., T'Joen, C., Canière, H., & De Paepe, M. (2013). Flow regime based calibration of a capacitive void fraction sensor for small diameter tubes. *International Journal of Refrigeration, 36*(2), 390-401.

dos Reis, E., & Goldstein, L. (2005). A procedure for correcting for the effect of fluid flow temperature variation on the response of capacitive void fraction meters. *Flow Measurement and Instrumentation, 16*(4), 267-274.

Elkow, K. J., & Rezkallah, K. S. (1996). Void fraction measurements in gas-liquid flows using capacitance sensors. *Measurement Science and Technology, 7*(8), 1153.

Feja, S. (2012). Measurement of electrical properties of refrigerants and refrigerant–oil mixtures. *International Journal of Refrigeration, 35*(5), 1367-1371. doi:https://doi.org/10.1016/j.ijrefrig.2012.03.011

Geraets, J., & Borst, J. (1988). A capacitance sensor for two-phase void fraction measurement and flow pattern identification. *International Journal of Multiphase Flow, 14*(3), 305-320.

Haynes, W. M. (2014). *CRC handbook of chemistry and physics*: CRC press.

Isbin, H. S., Sher, N. C., & Eddy, K. C. (1957). Void fractions in two-phase steam-water flow. *AIChE Journal, 3*(1), 136-142. doi:10.1002/aic.690030122

Jaworek, A., & Krupa, A. (2004). Gas/liquid ratio measurements by rf resonance capacitance sensor. *Sensors and Actuators A: Physical, 113*(2), 133-139.

Jaworek, A., & Krupa, A. (2010). Phase-shift detection for capacitance sensor measuring void fraction in two-phase flow. *Sensors and Actuators A: Physical, 160*(1), 78-86.

Jaworek, A., Krupa, A., & Trela, M. (2004). Capacitance sensor for void fraction measurement in water/steam flows. *Flow Measurement and Instrumentation, 15*(5), 317-324.

Kendoush, A. A., & Sarkis, Z. A. (1995). Improving the accuracy of the capacitance method for void fraction measurement. *Experimental Thermal and Fluid Science, 11*(4), 321-326.

Keska, J. K., Smith, M. D., & Williams, B. E. (1999). Comparison study of a cluster of four dynamic flow pattern discrimination techniques for multi-phase flow. *Flow Measurement and Instrumentation, 10*(2), 65-77.

Koyama, S., Lee, J., & Yonemoto, R. (2004). An investigation on void fraction of vapor–liquid two-phase flow for smooth and microfin tubes with R134a at adiabatic condition. *International Journal of Multiphase Flow, 30*(3), 291-310. doi:https://doi.org/10.1016/j.ijmultiphaseflow.2003.10.009

Olivier, S., Meyer, J., Elton, L., Müller, C., Martin, S. J., Huisseune, H., . . . Marzo, S. (2015). Measured void fraction and heat transfer coefficients during condensation. *Sort, 100*, 250.

Olivier, S. P., Meyer, J. P., De Paepe, M., & De Kerpel, K. (2016). The influence of inclination angle on void fraction and heat transfer during condensation inside a smooth tube. *International Journal of Multiphase Flow, 80*, 1-14.

Schmidt, J., Giesbrecht, H., & van der Geld, C. W. M. (2008). Phase and velocity distributions in vertically upward high-viscosity two-phase flow. *International Journal of Multiphase Flow, 34*(4), 363-374. doi:https://doi.org/10.1016/j.ijmultiphaseflow.2007.10.013

Sedrez, P. C., & Barbosa, J. R. (2015). Relative permittivity of mixtures of R-134a and R-1234yf and a polyol ester lubricating oil. *International Journal of Refrigeration, 49*(Supplement C), 141-150. doi:https://doi.org/10.1016/j.ijrefrig.2014.09.019

Wojtan, L., Ursenbacher, T., & Thome, J. R. (2004). Interfacial measurements in stratified types of flow. Part II: Measurements for R-22 and R-410A. *International Journal of Multiphase Flow, 30*(2), 125-137. doi:https://doi.org/10.1016/j.ijmultiphaseflow.2003.11.009

Wojtan, L., Ursenbacher, T., & Thome, J. R. (2005). Measurement of dynamic void fractions in stratified types of flow. *Experimental Thermal and Fluid Science, 29*(3), 383-392. doi:https://doi.org/10.1016/j.expthermflusci.2004.05.017

Yashar, D. A., Wilson, M. J., Kopke, H. R., Graham, D. M., Chato, J. C., & Newell, T. A. (2001). An Investigation of Refrigerant Void Fraction in Horizontal, Microfin Tubes. *HVAC&R Research, 7*(1), 67-82. doi:10.1080/10789669.2001.10391430